Impedance Transformers for High Frequency Molecular Electronics

Jonah Waissman

Under the supervision of
Professor Andreas Wallraff

Quantum Device Lab
ETH Zurich

December 27, 2006

Abstract

Improvements in the performance of electronic devices are largely based on the continued miniaturization of electronic components. To circumvent physical limits inherent in silicon technologies, single molecules may be used for the development of nanoscale electronics. To characterize molecular devices, measurements of their electrical transport properties must be performed. The high impedances of molecular devices, on the order of the quantum resistance and above, limit the speed with which measurements may be performed. Measurement resolution can be increased to nanosecond time scales by embedding the molecule in a high frequency resonant circuit, an increase of several orders of magnitude over low frequency measurements. Sensitivity can be optimized by impedance matching to the molecule. In this project, high frequency impedance transformation circuits for molecules or other nanoscale quantum electronic systems are investigated. Results on experimental realizations of lumped and distributed element PC Board impedance transformers are reported. The reactive and loss components limiting high bandwidth operation for large impedances are identified. To reduce losses, low temperature measurements are performed for distributed element circuits. For ultra-low loss operation with superconductors, a device layout for optical or electron beam lithography is designed, and considerations for future quantum device integration are described.

Contents

1 Introduction

1.1 Molecular Electronics

What is molecular electronics? This question turns out to be a deep one that may be approached in many ways. Let us begin with the name.

Fundamentally, the term "electronic" refers to the use of electrons, and "electronic" devices are those that are characterized by their transport of electrons. How is this characterization carried out? Again the answer is intuitive: by hooking up two metal leads to the device and then reading out its resistance on an ohmmeter. Then electromagnetic theory, in particular Ohm's Law $V = IR$, tells everything one needs to know about how much current flows through the device when a voltage is applied, or vice versa. This is made useful with the creation of a transistor: an electrical element whose resistance is controlled by an electrical parameter, such as a voltage gate.

"Molecular", of course, refers to molecules, the most basic combinations of atoms that together form all the kinds of matter seen in the natural world. "Molecular electronics" is therefore the use of molecules themselves as electronic devices.

Let us now consider the question of molecular electronics from another perspective. The semiconductor industry, based on transistors operating in silicon, has for years been following Moore's Law, which states that the number of transistors on a chip doubles approximately every 18 months. This trend has been followed closely until almost the present day. The reason for doing so rests on sound scientific and economic principles: chips with a greater number of smaller transistors are faster and more powerful.

Things can only get so small, however, and the limits of Moore's Law rests with the laws of physics. At the nanoscopic scales necessary for the further miniaturization of transistors, silicon technology is no longer capable of sustaining the trend.

The question of molecular electronics now appears to be, in fact, quite relevant. They are small and could potentially consume less power in a commercial application compared to current technologies. Thus molecular electronics has an intrinsic scientific and technological importance to be explored.

Since molecules are so small, however, another legitimate question may be asked: just how exactly does one attach an ohmmeter to a single molecule? This question cannot be answered so quickly; a variety of scientific work has been conducted in an attempt to do so [1]. In what follows, the current approaches are summarized, and the goals of the project described in this report are explained.

1.1.1 Current Approach

A variety of approaches to the problem of electronically accessing molecules have been developed [1]. In one technique, the molecules lie scattered on a gold

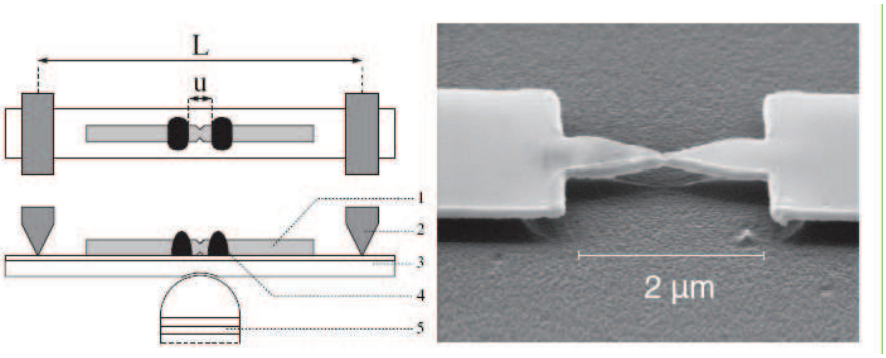

Figure 1: Left: top view and cross-section of the mechanically-controlled break junction with (1) gold nanowire with thinned region, (2) counter supports, (3) bending beam, (4) epoxy adhesive, (5) piezoelectric pushing rod. Right: Electron micrograph of a lithographically fabricated MCBJ made of Co with metal thickness 150 nm. *Picture credit: J. van Ruitenbeek et al.*

substrate, and the tip of a scanning tunneling microscope (STM) is used to pick up one end of the molecule, leading to an electronic connection. Another technique utilizes a substrate filled with holes, which lies on gold. The molecules are placed inside the holes leading to a connection on one end, and then capped with a gold particle, allowing for an electronic connection with an STM.

The technique that this report shall be referring to, however, is a more direct approach, in essence attempting to fabricate the leads for a resistance, or conductance, measurement. In this technique, a gold nanowire is formed, with a small thinned portion. The thinned portion is then broken; this can be accomplished by: 1) the nanowire is held down on both ends and pushed up from the center via a piezoelectric pushing rod, causing the thinned portion to break, known as a mechanically controlled break junction (MCBJ) (see Fig. 1); 2) a current is sent through the nanowire in a controlled fashion, i.e. negative feedback control, such that the crystal lattice of the thinned portion experiences a mechanical force and, with the right amount of current, electromigrates, essentially blowing open like a fuse and forming an electromigrated break junction with typical separations of 1 nm [3].

With the break junction, or nanogap, formed, what is left is to place a molecule inside. The basic method is to apply a droplet of a solution containing the desired molecule over the area of the nanowire (see Fig. 1, left panel). Clearly, the process of molecule attaching to leads is probabilistic, and may result in the desired one-molecule configuration, but problems may arise inside the gap: multiple molecules, other undesired molecules, various orientations of the molecules, and filaments of the original nanowire. In each case, the electrical properties measured will not be that of the desired single molecule in the proper orientation. To improve the chances of a proper connection, thiol groups which bond strongly to gold may be chemically attached to the ends of the molecule

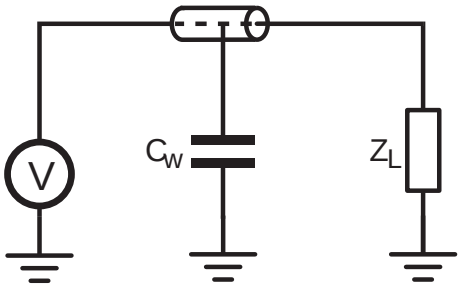

Figure 2: A typical setup for DC measurement of molecular electronics and other quantum systems. A voltage V is applied through a wire with stray capacitance C_W to a resistive load Z_L.

under study.

It is shown that a variety of issues are presented to the scientist wishing to experiment with molecular electronics. Let us now examine a separate issue, independent of the particular setup at the nanogap itself. The following section will explore the DC measurement setup assumed throughout the above experiments and demonstrate the limitations of such a setup.

1.1.2 Limitations of the DC Technique

Figure 2 illustrates a simplified typical setup for DC measurement of molecular electronics experiments. In this setup, a voltage V is applied through a transmission line with stray capacitance C_W to a load Z_L. For now, Z_L is assumed to be purely resistive, and will be referred to as $\mathrm{Re[Z_L]}$; more general cases will be considered later. The measurement typically done is to place a large current bias resistor in series with the load $\mathrm{Re[Z_L]}$ and read the current induced, thus extracting information about the conductivity of the load. Note that $\mathrm{Re[Z_L]}$ is large, since ideally a minimum number of conductance channels (i.e. a single molecule) are open, requiring a much larger bias resistor.

The stray capacitance C_W, present in all wires, forms along with the load $\mathrm{Re[Z_L]}$ an RC circuit with associated characteristic time constant $\tau = \mathrm{Re[Z_L]C_W}$. The characteristic time constant τ defines the time scale on which the voltage drop across the load $\mathrm{Re[Z_L]}$ can change. In other words, if at voltage $V = V_0$ there is a voltage drop V_L across $\mathrm{Re[Z_L]}$, then when another voltage $V = V_1$ is applied $\mathrm{Re[Z_L]}$ will take at least the time τ to exhibit a second voltage drop V_L'. Thus τ defines a bandwidth given by

$$BW \equiv (2\pi\tau)^{-1} = \frac{1}{2\pi \mathrm{Re[Z_L]C_W}}. \tag{1}$$

This bandwidth is the frequency at which $\mathrm{Re[Z_L]}$ can respond to a change in applied voltage. Thus BW places an upper limit on the frequency at which different voltages may be applied to probe $\mathrm{Re[Z_L]}$.

Typically, C_W is on the order of 100 pF for a 1 meter long line. If $\mathrm{Re}[\mathrm{Z_L}] = 10$ kΩ, the order of the quantum resistance $\hbar/2e^2$, then $\tau = 10^{-6}$ seconds and $BW \approx 150$ kHz. Single molecules have been shown to exhibit resistances on the order of 1 MΩ, giving $BW \approx 1.5$ kHz.

This bandwidth is, in fact, limited: it is possible to improve this by several orders of magnitude by replacing the DC measurement setup with a sensitivity-optimized high frequency technique. In such a technique, the bandwidth is a function of parameters set by the measurement circuit design, and thus can be optimized for fast response times on the order of nanoseconds. In addition, these techniques apply not only to molecular electronics but to studies of other quantum systems, which share the characteristic of a high load impedance leading to slow response times.

1.2 High Frequencies

The issue of limited response time inherent in current DC methods of molecular electronics can be effectively eliminated by moving from DC to high frequency, microwave measurements. In the microwave regime, rather than measuring $I - V$ curves, the quantity of measurement is the reflection coefficient Γ of a resonant circuit attached to the molecule. By sending voltage waves towards the circuit and reading their reflections with Γ, a change in the conductance of the molecule can be registered as a change in the resonance of the microwave circuit. In such a circuit, the quality factor Q is defined as

$$Q \equiv \frac{\omega_0}{BW}, \tag{2}$$

where ω_0 is the resonance frequency and BW is the bandwidth. Therefore,

$$BW = \frac{\omega_0}{\mathrm{Q}}, \tag{3}$$

and thus for a particular resonant circuit with a fixed Q, we increase the bandwidth by increasing the operating resonance frequency. In addition, the sensitivity of Γ is shown to be optimized when the characteristic input line impedance Z_0 is matched to the desired match load Z_L^0, where the load is the molecule under study. The following sections describe the theoretical background necessary for microwave measurement of the reflection coefficient Γ of a high frequency microwave circuit.

1.2.1 The Reflection Coefficient

Transmission line theory examines the propagation of voltage and current waves along long strips of conductors. When constructing the wave solutions to Maxwell's equations, the general form is expressed as

$$V(x) = Ae^{-ikx} + Be^{ikx} \tag{4}$$

where k is the spatial frequency of the wave, A is the amplitude of forward-traveling waves, and B is the amplitude of backwards-traveling waves. This can be reexpressed as

$$V(x) = A\left(e^{-ikx} + \Gamma e^{ikx}\right) \tag{5}$$

where A is now an arbitrary amplitude constant and $\Gamma \equiv B/A$ is the reflection coefficient, which relates the amount of backwards-traveling waves present in the signal of spatial frequency k.

The current in this transmission line is given by

$$I(x) = \frac{A}{Z_0}\left(e^{-ikx} - \Gamma e^{ikx}\right) \tag{6}$$

where Z_0 is the characteristic impedance of the transmission line. A position-dependent impedance along the transmission line can now be defined as

$$Z(x) \equiv \frac{V(x)}{I(x)}. \tag{7}$$

One would now like to examine the case of a transmission line with a load Z_L attached [4]. The load Z_L is considered to be purely resistive, unless otherwise stated (the general case, of stray reactive components in the load, is considered later). To do so, the position variable x is defined to be zero at the position of the load, and $-l$ at the input end of the transmission line, where l is the length of the transmission line. By Eq. 7 the position-dependent impedance $Z(x)$ at the load Z_L is then found to be

$$Z(0) = Z_L = \frac{1+\Gamma}{1-\Gamma} Z_0. \tag{8}$$

Rearranging for the reflection coefficient Γ gives

$$\Gamma(\omega) = \frac{Z_L(\omega) - Z_0}{Z_L(\omega) + Z_0}. \tag{9}$$

The limiting values of the reflection coefficient can be extracted from Eq. 9. The reflection coefficient is maximized ($|\Gamma| = 1$) in the two cases $Z_L = 0$ and $Z_L = \infty$. It is minimized ($|\Gamma| = 0$) when $Z_L = Z_0$. Z_L is then said to be matched to Z_0, and no reflections happen at the line-load interface.

Figure 3 shows the magnitude and phase of the reflection coefficient Γ. There is one point of note, where $Z_L = Z_0$ and the load is matched. Here, both the magnitude and phase of Γ are undergoing maximum change with respect to the load. Note that the rest of this report will plot only the magnitude of Γ for clarity and brevity; the phase could just as well be used. Thus to maximize the sensitivity of the measurement, where sensitivity is defined as $\partial\Gamma \backslash \partial Z_L$, the load Z_L must be matched to the input line. We now desire to know the method necessary to achieve, for an arbitrary load Z_L^0 (the molecule or other quantum system), the matched condition.

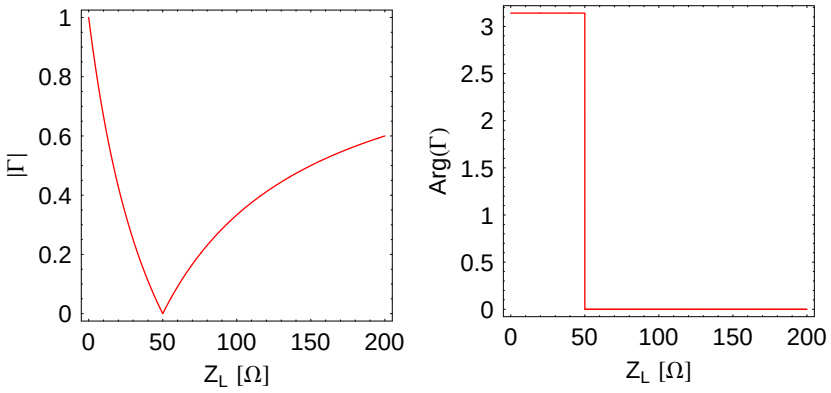

Figure 3: The reflection coefficient Γ plotted for real loads Z_L and $Z_0 = 50\ \Omega$. Left: Magnitude of the reflection coefficient $|\Gamma|$. Right: Phase of the reflection coefficient $\text{Arg}(\Gamma)$.

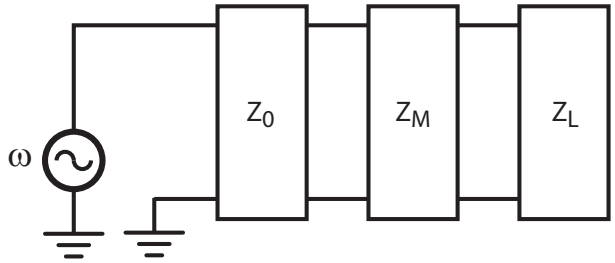

Figure 4: The generalized matching problem: A transmission line of characteristic impedance Z_0 must be matched to a load Z_L using an impedance Z_M.

1.2.2 The Matching Problem

The general problem of matching an impedance Z_L to a line impedance Z_0, shown in Fig. 4, is in theory relatively simple. The first condition to obtain a match is that at some frequency ω_0, the electrical length of Z_M is such that reflected waves experience destructive interference. Thus if Z_M has a physical length l_M,

$$\beta_0 l_M = \frac{\pi}{2} \tag{10}$$

where

$$\beta_0 = \frac{\omega_0}{v_p} \tag{11}$$

and v_p is the electromagnetic velocity of propagation in Z_M. Thus Z_M is termed a quarter-wave transformer.

To execute the match, the input impedance of a transmission line with electrical length $\pi/2$ and characteristic impedance Z_M with load Z_L attached is

equated to Z_0. This gives the second matching condition

$$Z_0 = Z_M \frac{Z_L + \imath Z_M \tan \beta_0 l_M}{Z_M + \imath Z_L \tan \beta_0 l_M}. \tag{12}$$

The first condition sends the tangent terms to infinity; in this limit, we obtain

$$Z_M = \sqrt{Z_0 Z_L}. \tag{13}$$

That is, the matching impedance Z_M is the geometric mean of the load and line impedances.

In theory, then, the problem is solved. Take the desired Z_L, find the right Z_M, and a beautiful readings with high bandwidth and high sensitivity will result. Of course, science is never this simple, and here it is no different. The challenge is to design, construct, and realize an appropriately large Z_M for the high impedances of molecules and other quantum systems, and to do so while obtaining high bandwidth to enable fast measurements.

1.3 Goals of this Project

This project seeks to investigate different methods of fabricating impedance matching circuits. The goal is to perform measurements on two different room temperature PC Board impedance transformers, lumped element and distributed element circuits, and determine parameters that limit their high bandwidth, high frequency operation. Measurements investigating performance improvement at low temperatures are also performed. In addition, this project lays the groundwork for small-scale, low-temperature and low-loss impedance transformers with the design of a mask for optical or electron beam lithography, for the use of silicon chip-based transformers.

2 Lumped Element Transformers

The goal of the impedance matching problem is to fulfill two parameters: matching to a load Z_L^0 at a frequency ω_0. Thus the simplest solution will contain two degrees of freedom. This is satisfied by the most basic impedance transformer, the LC circuit. This section will describe the operation and characteristics of this circuit, as well as its experimental implementation and subsequent results obtained.

2.1 Theory

2.1.1 Design Equations

The lumped element impedance transformer is shown in Fig. 5. The impedance of the LC circuit is defined by the parallel combination of the load Z_L^0 and the

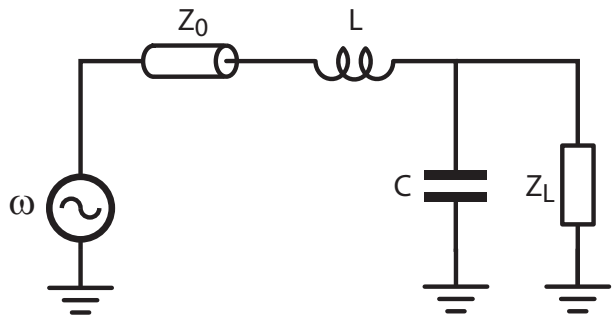

Figure 5: The lumped element impedance transformer: a voltage source at frequency ω is connected via a transmission line of characteristic impedance Z_0 to an inductance L and capacitance C, which match to the load Z_L^0.

capacitance C, in series with the inductance L and the transmission line. Again, Z_L^0 is considered to be purely resistive. The input impedance is thus written as

$$Z_{\text{in}} = \imath\omega L + \left(\imath\omega C + \frac{1}{Z_L^0}\right)^{-1}. \tag{14}$$

Utilizing the match condition

$$Z_{\text{in}} = Z_0, \tag{15}$$

and the resonance condition,

$$\omega_0 = \frac{1}{\sqrt{LC}}, \tag{16}$$

we fix the two degrees of freedom and can derive equations for the required inductance and capacitance in terms of the desired resonance frequency and matched load. These are given by

$$L = \frac{\sqrt{\frac{Z_L^0}{Z_0} - \frac{1}{2}}}{\omega_0 Z_L^0} \tag{17}$$

$$C = \frac{Z_L^0}{\omega_0 \sqrt{\frac{Z_L^0}{Z_0} - \frac{1}{2}}}. \tag{18}$$

The circuit parameters are now completely determined.

Figure 6 shows plots of the design equations versus the matched load Z_L^0. These demonstrate the behavior that will govern our choices of circuit components. To match to higher loads, higher inductances and lower capacitances are required. Both the inductance and capacitance decrease with higher operating frequency. Later it will be shown how this behavior imposes experimental limits.

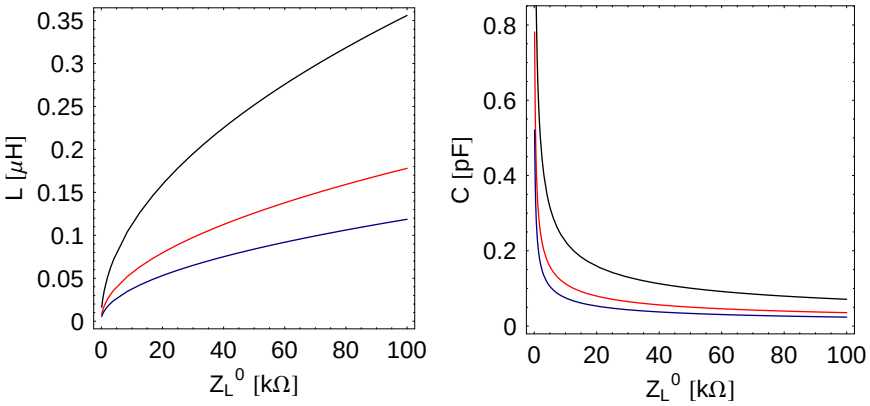

Figure 6: Left: Inductance L as a function of matched load Z_L^0. Right: Capacitance C as a function of matched load Z_L^0. In both: ω_0={black=1 GHz, red=2 GHz, blue=3 GHz}.

2.1.2 Reflection Coefficient

The measured quantity of the matching circuit and load will be the reflection coefficient Γ. Equation (9), the definition of Γ, allows us to calculate the reflection coefficient for the lumped element matching circuit with load as

$$\Gamma = \frac{\imath\omega L + \left(\imath\omega C + \frac{1}{Z_L}\right)^{-1} - Z_0}{\imath\omega L + \left(\imath\omega C + \frac{1}{Z_L}\right)^{-1} + Z_0} \tag{19}$$

Figure 7 illustrates the frequency dependence of the reflection coefficient for loads Z_L below and above the matched load Z_L^0, for a 10 kΩ match at 1 GHz. In the below match case, as the load decreases, the resonance broadens and moves towards lower frequencies, eventually disappearing. In the above match case, as the load increases, the resonance decreases towards the open circuit limit of no resonance. By attaching variable loads to experimental realizations of the lumped element transformer, we can thus test them for this matching behavior and confirm proper design.

To maximize measurement speed in the final measurement system, it is possible to take readings at a single frequency, rather than frequency spectra. One needs only to ensure that there is appropriate sensitivity to the load at the measurement frequency, i.e. that $\partial\Gamma\backslash\partial Z_L$ is appropriately large around Z_L^0, the matched load. Figure 8 demonstrates this behavior for this lumped element circuit. Decreasing and increasing the frequency off-match have a similar effect of sharply decreasing sensitivity around the matched load.

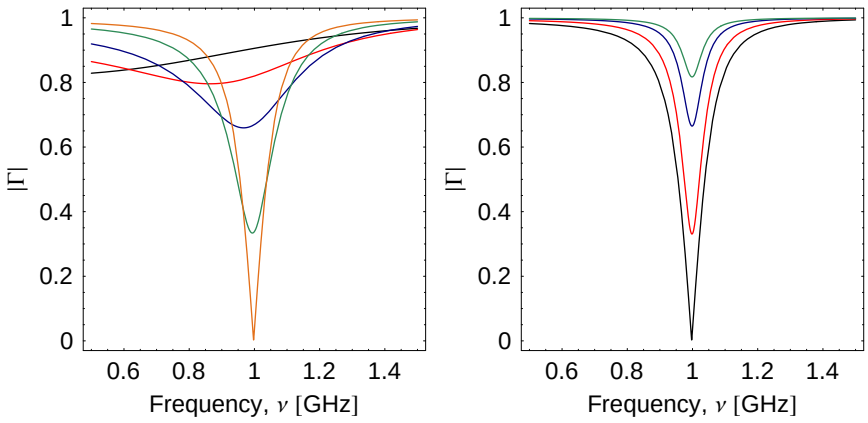

Figure 7: Reflection coefficient magnitude, $|\Gamma|$, versus frequency ν for loads around match. The matched load Z_L^0 is 10 kΩ. Left Panel: Loads below match. In kΩ: black=.5, red=1, blue=2, green=5, orange=10. Right Panel: Loads above match. In kΩ: black=10, red=20, blue=50, green=100.

2.1.3 Quality Factor

The quality factor of this circuit is derived from the definition of the quality factor as

$$Q \equiv \omega_0 \frac{\text{EnergyStored}}{\text{EnergyLostPerCycle}} \tag{20}$$

Using the equivalence of the magnetic and electric energies at resonance and considering the energy stored in a capacitor and the loss mechanism of the resistive load, one obtains

$$Q = \omega_0 Z_L C \tag{21}$$

The resonance condition then gives

$$Q = \frac{Z_L}{\sqrt{\frac{L}{C}}}. \tag{22}$$

Transmission line theory says that the denominator of Eq. (22) is the characteristic impedance of a transmission line with an inductance and capacitance per unit length of L and C, respectively. Thus we identify this denominator as the characteristic impedance of the impedance transformer. From the general matching problem considered in the Introduction, this is Z_M. Eq. (13) then gives

$$Q = \sqrt{\frac{Z_L}{Z_0}}. \tag{23}$$

This elegant result, particular to the lumped element case, will prove to be useful in understanding the relationship between quality factors of impedance transformers and their possible matched loads.

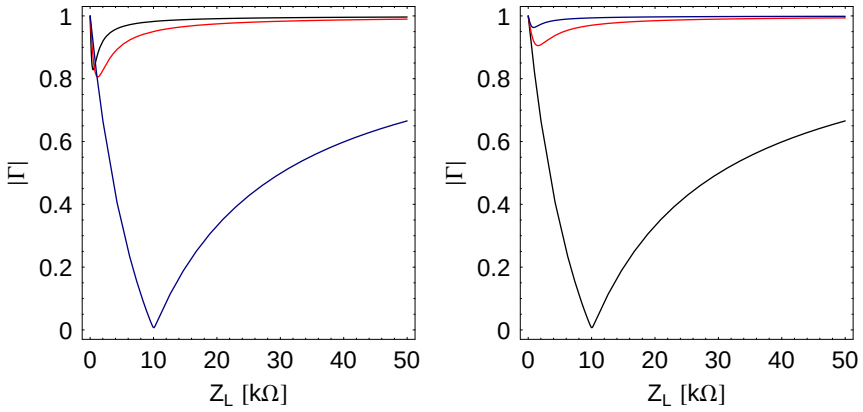

Figure 8: Reflection coefficient magnitude, $|\Gamma|$, versus load Z_L for frequencies around resonance. The matched load Z_L^0 is 10 kΩ. Left Panel: Frequencies below resonance. In GHz: black=.5, red=.75, blue=1. Right Panel: Frequencies above resonance. In GHz: black=1, red=1.25, blue=1.5.

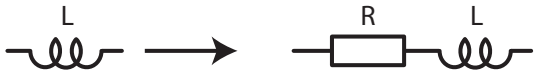

Figure 9: The model for resistive losses in the lumped element transformer consists of this substitution in the original, ideal design.

2.1.4 Internal Losses

In real circuits, internal losses of the circuit components and cabling play a non-negligible role. In the case of the lumped element impedance transformer, these losses can be modeled by the addition of a resistance R in series with the inductor, as illustrated in Fig. 9.

Figure 10 demonstrates the effect of internal losses on the reflection coefficient. In the frequency domain, losses push the resonance into the above-match regime. In the load domain, the match is also steadily worsened and sensitivity is lost around the desired match load of 10 kΩ.

Since Eq. (23) relates the impedance transformation ratio to the Q of the circuit, it is important to understand the effect of losses on the Q since these will alter both possible matched loads and bandwidths. The simple cases of fully parallel or series LRC circuits are easily treated by considering the form of the parallel Q given in Eq. (21) and its series version

$$Q_{\text{series}} = \frac{1}{\omega_0 Z_L C}. \tag{24}$$

By considering the total resistance of either a parallel LRC with parallel loss

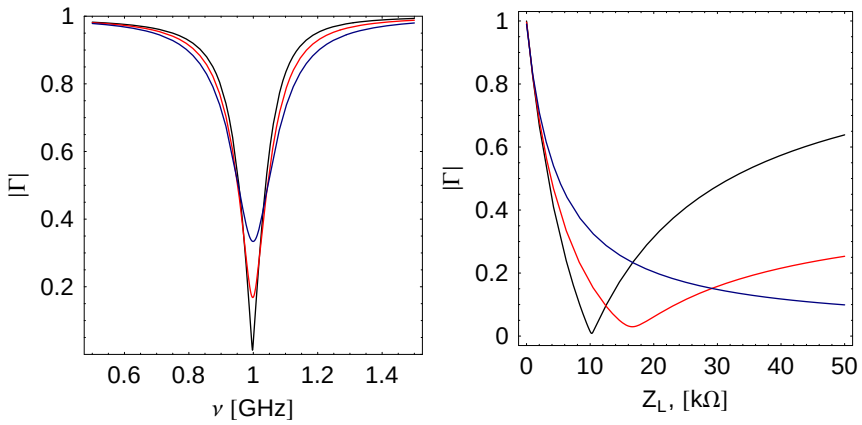

Figure 10: Left Panel: Reflection coefficient magnitude $|\Gamma|$ versus frequency ν. Nominal match: 10 kΩ at 1GHz. Right Panel: Reflection coefficient magnitude, $|\Gamma|$ versus load Z_L. Nominal match: 10 kΩ at 1GHz. Both panels have a series loss resistance R in Ω given by: black=1, red=20, blue=50.

or a series LRC with series loss, it is seen that in both cases,

$$\frac{1}{Q_{\rm tot}} = \frac{1}{Q_{\rm ext}} + \frac{1}{Q_{\rm int}}, \tag{25}$$

where $Q_{\rm tot}$ is the total Q, $Q_{\rm ext}$ is the external Q given by the desired load, and $Q_{\rm int}$ is the internal Q arising from the combination of the LC and the internal loss component R. Thus, the Q's add in parallel for these simple cases.

Equation 25 provides an important perspective on the resonance process. For a fixed $Q_{\rm ext}$,

$$Q_{\rm int} \gg Q_{\rm ext} \Rightarrow Q_{\rm tot} \approx Q_{\rm ext} \tag{26}$$

$$Q_{\rm int} \ll Q_{\rm ext} \Rightarrow Q_{\rm tot} \approx Q_{\rm int}. \tag{27}$$

Thus it is shown that higher internal quality factors are desirable for a good measurement of the external Q.

For the case of the lumped element impedance transformer, the match load Z_L^0 adds in parallel to the transformer but the internal loss R adds in series. To determine the total dissipative contribution to the circuit impedance, we find the real part of the input impedance of the lossy transformer, given by

$$\mathrm{Re}[\mathrm{Z_{in}}] = \mathrm{R} + \frac{\mathrm{Z_L}}{1 + (\omega \mathrm{Z_L C})^2}. \tag{28}$$

This is the equivalent series resistance for the lumped element transformer. By fixing the impedance at the resonant frequency ω_0 the Q may now be written as in the series case as

$$\frac{1}{Q_{\rm tot}} = \omega_0 CR + \frac{\omega_0 Z_L C}{1 + (\omega_0 Z_L C)^2}. \tag{29}$$

Figure 11: An example of the lumped element transformer on a PC Board. From left to right, note the SMA connector with compensating structure, microstrip line, SMD inductor, and capacitive pad.

Rewriting using the parallel and series Q one thus obtains

$$\frac{1}{Q_{\text{tot}}} = \frac{1}{Q_{\text{int}}} + \frac{Q_{\text{ext}}}{1+Q_{\text{ext}}^2}, \tag{30}$$

where

$$Q_{\text{int}} \equiv \frac{1}{\omega_0 RC} \tag{31}$$

$$Q_{\text{ext}} \equiv \omega_0 Z_L C. \tag{32}$$

In the case of large external Q, or by Eq. (23) large matched loads, as this project is interested in, Eq. (30) reduces to

$$\frac{1}{Q_{\text{tot}}} \approx \frac{1}{Q_{\text{int}}} + \frac{1}{Q_{\text{ext}}}, \tag{33}$$

and thus in the regime of interest the total Q of the lumped element transformer circuit is a parallel combination of the internal and external Q's. Thus the same conditions for a good measurement of Q_{ext} apply as in the two simple LRC cases. By Eq. (23), we therefore require high internal Q's for higher loads, and thus small losses in the circuit components. The condition on small losses is given by Eq. (28), which shows that for the external dissipation to dominate,

$$R \ll \frac{Z_L}{1+(\omega_0 Z_L C)^2}. \tag{34}$$

2.2 Experiment

Experimental realizations of the lumped element impedance transformers for differing parameter values have been fabricated and tested. Their design, results and final considerations are elaborated upon below.

2.2.1 Design

The first tests of lumped element impedance transformers were performed on PC Board (PCB) consisting of 1.5 mm thick FR4 with 35 μm thick copper

Figure 12: The microstrip transmission line cross section, with center conductor width W, substrate height H, substrate relative dielectric constant ϵ_r, and center conductor thickness T.

metallization. Figure 11 displays the design. A coaxial cable is attached via an SMA connector to a 50 Ω matched microstrip line. Microstrip is a transmission line geometry defined by a strip of conductor of width W suspended at height H over a ground plane (Fig. 12). They are easy to fabricate on PCBs and exhibit convenient scaling on the PCB scale. The 50 Ω microstrip match is achieved by calculating the effective dielectric constant for the microstrip and the width for the chosen impedance of 50 Ω [4, 2]. Different transmission line geometries will be discussed further in the distributed element section. To reduce stray reactive components at the connector transition from SMA cable to microstrip, a compensating structure is used as recommended by the manufacturer [].

A pad lies at the end of the line for the soldering of the surface mount device, or SMD, inductor. Because high matched loads require low capacitances, it is unnecessary to attach an SMD capacitor to the circuit. Instead, the capacitance of the inductor soldering pad is used as the matching circuit C. To calculate the capacitance of this pad, Maxwell, a finite-element analysis program, was used. Maxwell allows the calculation of static electromagnetic fields in 2D and 3D geometries and capacitance matrix calculation. The pad capacitance can then be tailored to the particular requirement of a given load, frequency, and inductor.

For testing the matching circuit with a variable load impedance, a potentiometer with an appropriate resistance range for the chosen matched load Z_L^0 is soldered to the other end of the capacitive pad, as shown in Fig. 13. This potentiometer modifies the properties of the circuit, as will be discussed below.

To measure the DC resistance of the circuit and potentiometer, a bias tee is used as shown in Fig. 13. A bias tee is a three-terminal device with an RF input capacitively coupled to the output. The output is inductively coupled to the DC port. Thus it is possible to send RF signals to the output with isolation from DC signal while reading or sending DC signals through the DC port that are shielded from RF frequencies. A right-angle bend connector with an SMA-BNC adapter allows connection to an ohmmeter.

2.2.2 Fabrication

The PC Board circuits fabricated for all experiments in this report were designed in AutoCAD. To increase resolution, a scaled up printout is made of the design and a Repro machine is used to scale the print back down for exposure onto

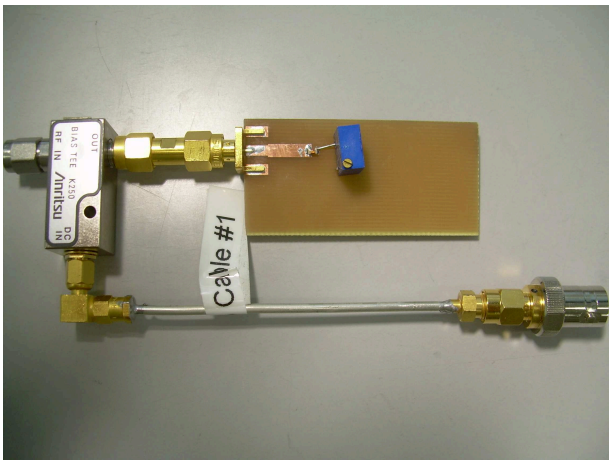

Figure 13: The measurement setup for the lumped element PC Board transformer. Note the potentiometer with trimmer and the bias tee. Also note the small size of the capacitive pad, with capacitance .13 pF for a match to 40 kΩ.

a negative film. The exposed negative is then developed onto a positive film, which is washed and dried. Care must be taken to obtain a proper exposure; typically, exposing slightly below the estimated value produces darker prints. A five minute UV exposure is performed with the positive film on the fully metalized PCB. The exposed PCB is then developed in solution, and wet-etched for ten minutes in a mixing chamber. After washing with acetone, the etched PCB is cut with a table saw according to design criteria. The ends are filed and the SMA connections are soldered onto the compensation structures.

2.2.3 Results

The following section discusses experimental results for an impedance transformer design with a nominal match of Z_L^0=5 kΩ operating at ν_0=1 GHz. This choice of match load for the fixed resonance frequency was based on an available SMD inductance value of 82 nH, whose choice will be explained later. The required capacitance for these parameters is .3 pF. As a zeroth order design calculation, a parallel-plate capacitor assumption was made to yield the dimensions for the capacitive pad.

Figure 14 shows a spectrum of an impedance transformer with a nominal match of 5 kΩ at 1 GHz in an open-circuit configuration. The first observation is that the frequency is shifted by nearly a factor of two to 600 MHz. To understand why this shift occurs, an electrostatic simulation was performed in Maxwell to determine a more accurate value for the pad capacitance. It yielded a pad-to-ground plane capacitance of .598 pF, about twice the approximated capacitance. Assuming the nominal SMD inductor value of 82 nH, this brings the resonance frequency to 700 MHz, explaining most of the shift.

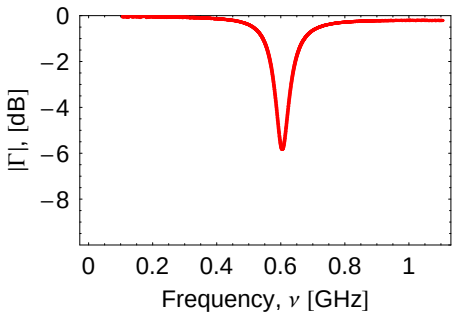

Figure 14: Experimental data on a lumped element impedance transformer with nominal match to Z_L^0=5 kΩ at ν_0=1 GHz, open-circuited.

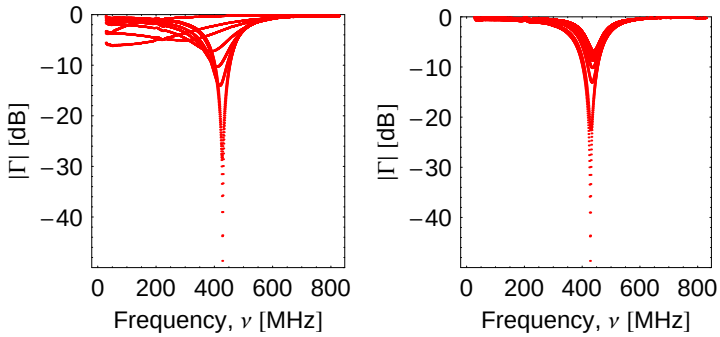

Figure 15: Experimental data on a nominal 5 kΩ match at 1 GHz with 20 kΩ potentiometer attached. Qualitatively, the correct behavior is observed. Actual match occurs at 1.66 kΩ. Load is varied: left=below match, right=above match.

A more accurate determination can be obtained by fitting the known analytic expression for the input impedance of the open-circuited transformer to the data. Because a resonance is observed even in the absence of an external load, the transformer must be matching to internal losses. The fit is thus performed to an open-circuited transformer that includes the loss component R previously discussed. The open-circuit fit is shown in the left panel of Fig. 16. This fit yields L_{eff}=120 nH, C_{eff}=.585 pF and R=15 Ω. The loss component is a reasonable number for an internal resistance. The capacitance remains similar to the calculated Maxwell value, but the effective inductance increases by 50%, indicating that this fit has possibly attributed all stray reactive components to the inductance. These values may then be used for more accurate modeling of impedance transformers with loads attached.

The quality factor of the open-circuited transformer is obtained with a Lorentzian fit in Mathematica and is calculated to be $Q_{\text{tot}} = 7.9$. The open-circuited impedance transformer is equivalent to one with $Z_L \to \infty$; by Eq. (21)

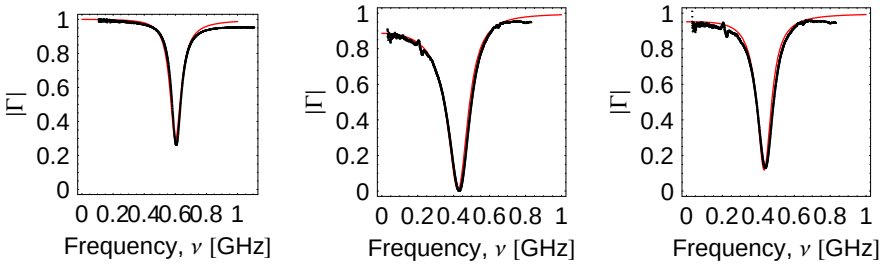

Figure 16: Analytic model fits to experimental data on lumped element resonances. Left: Open circuit. Center: On-match at 1.66 kΩ. Right: Off-match at 4 kΩ. All plots: black = data, red = analytic fit.

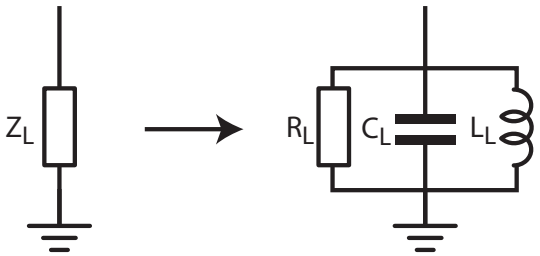

Figure 17: A schematic model of the reactive components in the potentiometer due to its construction characteristics. Note that in actuality the inductance is in series with the resistance, as in the analytic model discussed.

$Q_{\text{ext}} \to \infty$. Thus Eq. (27) places this measurement in the limit where $Q_{\text{tot}} \approx Q_{\text{int}}$ and therefore $Q_{\text{int}} \approx 8$.

Figure 15 shows experimental results for the same impedance transformer, now attached to a 20 kΩ potentiometer. The load is varied between Z_L=125 Ω and Z_L=18.7 kΩ, with actual match occurring at Z_L^0=1.66 kΩ. The qualitative behavior conforms closely to that predicted by the theory. Quantitatively, however, a lower resonance frequency than for the open load is observed as well as a lower match load than expected.

These secondary shifts have been attributed to the potentiometer. The variable load behavior it possesses is achieved by wrapping a long resistive wire into a coil and contacting this resistive coil at a fixed input contact and an output contact that lies at a varying position along its length. Varying this position varies the DC resistance. The solenoidal form of the wire, however, means it automatically possesses a large inductance. One may also conjecture that since the length of the solenoid is varied to vary the resistance, its inductance is thus a function of the measured DC resistance.

Fig. 17 shows a schematic of the potentiometer parasitics. Note that the following analytic model has the load in series with the potentiometer inductance.

Inductances, L [nH]	56	68	82	220	1130
Match Load at 1 GHz, Z_L^0 [kΩ]	2.4	3.6	5.3	38.2	1010
Capacitance for Z_L^0 at 1 GHz, C [pF]	.45	.37	.31	.12	.0224
Typ. $Q_{\rm int}$ of inductor (at 800MHz)	60	60	60	N/A	N/A
Min. Self-Resonant Frequency, SRF [MHz]	1700	1550	1430	950	350

Table 1: Properties of some available SMD inductor values at an operating frequency of 1 GHz.

The input impedance of the lossy lumped element transformer is then given by

$$Z_{\rm inPot.} = \imath\omega L + R + \left(\imath\omega C + \imath\omega C_L + \frac{1}{R_L} + \frac{1}{\imath\omega L_L}\right)^{-1} \tag{35}$$

Using the L, C, and R obtained from the open-circuit fit, this equation is fit to the potentiometer-loaded transformer data at the match load 1.66 kΩ and at an off-match load 4 kΩ. These are shown in the center and right panels, respectively, of Fig. 16. The match-load fit yields L_L=415 nH and C_L=.68 pF. The off-match fit yields L_L=2000 nH and C_L=.58 pF. The effective potentiometer capacitance is seen to be comparable to the original pad capacitance. The effective potentiometer inductance is large, and increases with increased load, as hypothesized. Thus the potentiometer strongly modifies the properties of the impedance transformer due to its construction.

While single molecules, the ultimate matching goal, will not have strays as large as potentiometers, the break junctions used to contact the molecules may carry stray reactive components due to the length of nanowire required and the nanogap formed by the leads. Hence while this analysis yields values not in line with what is ultimately expected, it is useful as a methodology to extract stray reactive components from loads of unknown character.

2.2.4 Limitations of Lumped Element Transformers on PC Boards

The limitations on lumped element circuits are determined by how large an inductance and how small a capacitance can be realized, and subsequently by the loss mechanisms in these components.

SMD inductors have parasitic impedances, which include dissipative and reactive components. Thus they exhibit not only inductance but also stray resistance and capacitance. Therefore the SMD inductors themselves have a resonant behavior. This leads to two crucial limits. The first is the internal Q of the inductor, which places an upper limit on the internal Q of the transformer. Table 1 displays, for several available SMD inductance values at an operating frequency of 1 GHz, the supported match load Z_L^0, required capacitance C for such a match, internal Q at 800 MHz and self-resonant frequency. For Z_L^0 approaching the kΩ regime, the internal Q's of the inductors reach 60. By Eq. (26) $Q_{\rm ext}$ is then limited to be much smaller than 60. If $Q_{\rm ext}$ must be ten

times less than Q_{int}, then by Eq. (26) the matched load $Z_L^0 < 2$ kΩ. This is dramatically below the matched loads of interest.

Below the resonance of the inductors, they will exhibit inductive impedance (i.e. $\imath\omega L$) but above it the impedance begins to decrease with frequency, exhibiting capacitive impedance (i.e. $1/\imath\omega C$). Transformer operation is therefore limited to be below this self-resonant frequency (SRF). Table 1 shows that for an operating frequency of 1 GHz at high matched loads of 1 MΩ, the SRF for available SMD inductors is in the low hundreds of megahertz. For Q's on the order of 10, as observed in these PCB circuits, this limits bandwidth to the dozens of megahertz, already too low to provide the high frequency advantages discussed in the introduction.

Since SMD capacitors are not used, the lower limit on capacitance is given by the size of the capacitive pad. In the PC Board case, this minimum is defined by the size of the inductor connection, which must be soldered to the pad, plus extra space to make the soldering physically feasible. This limit has been calculated with Maxwell to be approximately .13 pF. At this limit of PCB capacitance, $Z_L^0 \approx$40 kΩ and the SRF<1 GHz. In the range of measured Q_{tot}'s, the bandwidth is then limited to a hundred MHz or less.

In sum, the capacitive pad size limit sets an upper limit on the match load Z_L^0, the necessary inductor at this limit restrains Q_{tot} and the maximum operating frequency, by which the bandwidth is then also limited. PC Board lumped element matching circuits therefore will not be able to satisfy the requirements for high frequency molecular electronics, but have provided a useful testbed environment.

3 Distributed Element Circuits

As an alternative to discrete elements and their issues with internal losses, impedance transformers may be fabricated with variable lengths of transmission line. Such circuits are known as continuous or distributed element circuits. Their advantage is the avoidance of large loss and reactive components from surface mount devices and the enabling of high-frequency operation. This section discusses theoretical and experimental results on the use of these distributed element impedance transformers.

3.1 Theory

3.1.1 Single Stub Tuners: Lossless Lines

The single stub tuner is a design that takes advantage of the length-dependent input impedance of a transmission line. The strategy for the distributed element matching circuit is to select a length of transmission line a distance d from the attached load Z_L such that the input *admittance* is the characteristic admittance $Y_0 \equiv 1/Z_0$ plus an imaginary part, the susceptance B. A stub, or transmission line of length l, is then chosen to be attached in parallel to the original line at

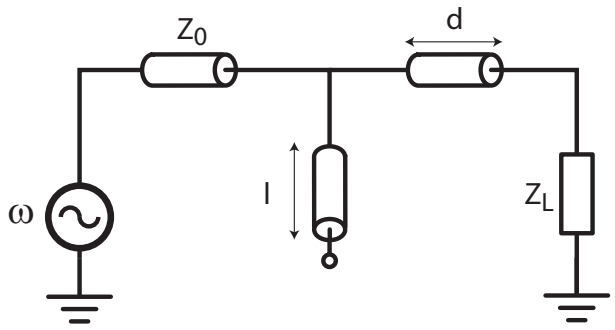

Figure 18: A single stub tuner. All transmission lines have characteristic impedance Z_0. The length d of transmission line is chosen along with the length l of the stub to cause the input impedance at the junction to be Z_0, the matching condition.

the point d. Since admittances add in parallel, the stub length l can be chosen to cancel the susceptance B, leaving the matched impedance Z_0.

The length-dependent input impedance of an ideal transmission line is given from basic transmission line theory as

$$Z_{\text{in}}(l) = Z_0 \frac{Z_L + \imath Z_0 \tan \beta l}{Z_0 + \imath Z_L \tan \beta l}, \tag{36}$$

where Z_0 is the characteristic impedance of the transmission line, Z_L is the attached arbitrary load impedance, l is the line length, and β is the spatial frequency, given by

$$\beta = \frac{\omega}{v}, \tag{37}$$

where ω is the operating frequency and v is the propagation velocity in the transmission line, defined from electrodynamics as

$$v = \frac{1}{\sqrt{\mu_0 \varepsilon_0 \varepsilon_{\text{eff}}}}. \tag{38}$$

ε_{eff} is the effective dielectric constant, defined by the particular transmission line geometry; this is discussed in a forthcoming section.

With a load Z_L attached to a transmission line of length d, as in Fig. 18, d is now chosen such that the admittance of the loaded input branch is $Y_0 + \imath B$, where $Y_0 \equiv 1/Z_0$. This condition fixes d.

A stub, or piece of transmission line of length l, is then attached in parallel at the point d, see Fig. 18. This stub is left open-circuited, such that its input impedance is

$$Z_{\text{stub}} = -\imath Z_0 \cot \beta l. \tag{39}$$

The stub length l can then be chosen such that the purely susceptive admittance of the stub precisely cancels the susceptance B of the original line of length d.

The input impedance at the junction of the line and stub will then be only the characteristic impedance Z_0, leading to a matched condition. A detailed derivation is given in [4].

For the case of a purely resistive load, the distance from the load d and the stub length l are given by

$$d = \frac{v}{\omega_0} \arctan \sqrt{\frac{Z_L^0}{Z_0}} \tag{40}$$

$$l = \frac{\lambda_0}{2} - \frac{v}{\omega_0} \arctan \frac{Z_L^0 - Z_0}{\sqrt{Z_L^0 Z_0}}, \tag{41}$$

where Z_L^0 is the desired matched load and $\lambda_0/2$ is the half-wavelength at the resonance ω_0 given by

$$\frac{\lambda_0}{2} = \pi \frac{v}{\omega_0}. \tag{42}$$

In the limit $Z_L^0 \gg Z_0$, these equations show that d grows and l decreases until both approach $\lambda_0/4$. This is due to the resonant nature of the circuit: the line length d is chosen slightly below the resonance while the stub length l is chosen slightly above, leading one to exhibit a capacitive impedance (the line input impedance $1/(Z_0 + \imath B)$) and the other an inductive impedance (the stub input impedance $\imath/B$). One can thence understand the single stub tuner at match as a resonator where one branch represents the inductor and the other a capacitor.

Both the line and stub length are inversely proportional to the chosen operating frequency. Thus for higher operating resonant frequencies we require shorter branches. However, the difference in length between the line and stub are also inversely proportional to frequency, as well as decreasing with higher chosen load. Therefore real-world designs will have to involve fabrication techniques with high resolution and reproducibility. Errors in line or stub length will lead to stray reactive components in the circuit.

3.1.2 Impedance and Reflection Coefficient

An analytic approach to analysis of the single stub tuner is possible by considering a parallel combination of transmission line input impedances. Writing down the input impedance of a transmission line of length d attached to a load Z_L in parallel with an open-circuit stub of length l, one obtains

$$Z_{\text{in}} = Z_0 \left(\frac{Z_0 + \imath Z_L \tan \beta d}{Z_L + \imath Z_0 \tan \beta d} + \imath \tan \beta l \right)^{-1}. \tag{43}$$

Eq. (9) now allows the calculation of the reflection coefficient.

Figure 19 shows the reflection coefficient $|\Gamma|$ around the chosen operating frequency ν_0=2 GHz for the single stub tuner impedance transformer, for a matched load Z_L^0=10 kΩ. The behavior is similar to the lumped element case:

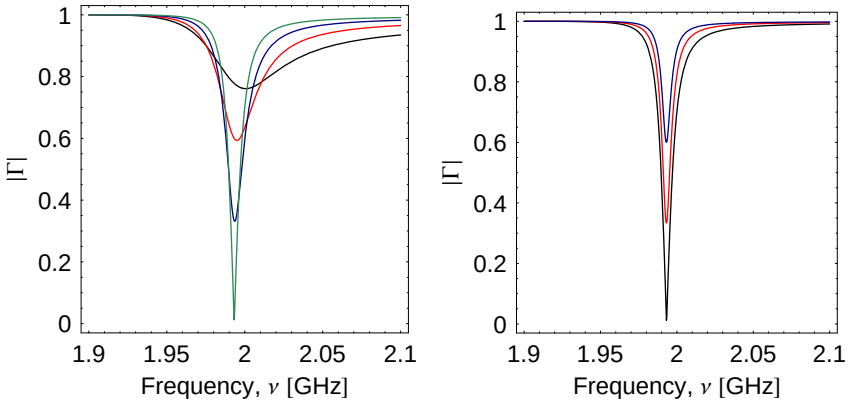

Figure 19: Analytic reflection coefficient of the $Z_L^0 = 10\ 10$ kΩ, $\nu_0 = 2$ GHz matching circuit. Left: loads below match; $Z_L = \{1.25, 2.5, 5, 10\}$ kΩ, match=green. Right: loads above match; $Z_L = \{10, 20, 40\}$ kΩ, match=black.

for loads below match, the reflection coefficient decreases until the resonance disappears (although at increasing frequency), while for loads above match the reflection coefficient increases towards the infinite-load limit of no resonance. The left panel of Fig. 20 shows the reflection coefficient for the same transformer, plotted against load Z_L. As in the lumped element case, moving off the operating frequency diminishes sensitivity around the matched load Z_L^0=10 kΩ.

The right panel of Fig. 20 shows the reflection coefficient plotted over a wider frequency range. Higher harmonics, a special property of distributed element transformers, are now visible. Altering the load Z_L now affects all harmonics, and thus the entire frequency range. In principle, transformer operation could happen at any one of the matched harmonics; in practice, frequency-dependent losses, which are typically higher at higher frequencies, prevent higher-harmonic operation. This will be discussed further in the proceeding section.

3.1.3 Lossy Transmission Lines

Real transmission lines are not ideal transmitters of electrical energy but have a number of loss mechanisms associated with them. These include losses in the conducting material, such as skin depth, scattering of electrons by lattice vibrations (phonons), impurities, defects, and surface roughness, as well as losses in the surrounding dielectric. It is possible to consider lossy transmission lines by applying to the distributed element circuit impedance equations the algebraic mapping

$$\imath \tan \beta l \rightarrow \tanh \gamma l \tag{44}$$

where γ is the lossy propagation constant defined as

$$\gamma \equiv \alpha + \imath\beta \tag{45}$$

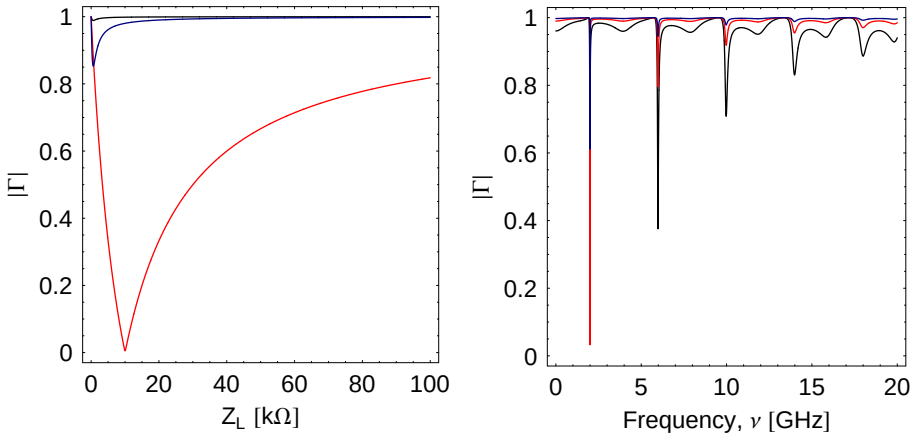

Figure 20: Magnitude of the reflection coefficient $|\Gamma|$ for the ideal distributed element impedance transformer, matched to $Z_L^0 = 10$ kΩ at $\nu_0 = 2$ GHz. Left: versus load Z_L, for frequencies $\nu = \{\nu_0$ (red), $\nu_0 + .05$ GHz (blue), $\nu_0 - .05$ GHz (black)$\}$. Right: versus frequency ν, over a wider frequency range showing higher harmonics, for $Z_L = \{Z_L^0$ (red), $4Z_L^0$ (blue), $Z_L^0/4$ (black)$\}$.

with β the lossless propagation constant and α the lossy attenuation constant. In the case α=0, the original lossless behavior is recovered [4].

The left panel of Fig. 21 shows the effect of a constant, frequency-independent α on the reflection coefficient $|\Gamma|$ in the frequency domain of a transformer matched to Z_L^0=10 kΩ at ω_0=2 GHz. The effect is to increase $|\Gamma|$ and reduce the match. In the same figure, the right panel shows the effect of α, again constant and frequency-independent, on $|\Gamma|$ in the load domain. The sensitivity is rapidly diminished as α increases. This demonstrates that a realized distributed element impedance transformer must have a small α for good sensitivity.

The attenuation constant α, as mentioned earlier, has many physical mechanisms associated with it. Design equations describing the functional dependence of these loss mechanisms on parameters such as the geometry of the transmission line, its physical characteristics, and its operating parameters have been developed. These are available in [2, 6]. In general, these loss mechanisms are frequency dependent and increase with increasing frequency. These will be described further in the experimental section.

3.2 Experiment

3.2.1 Design

Figure 22 shows a realized PC Board distributed element impedance transformer. The SMA connector at left is connected to the PC Board via its appropriate manufacturer-supplied compensation structure to minimize stray reactive

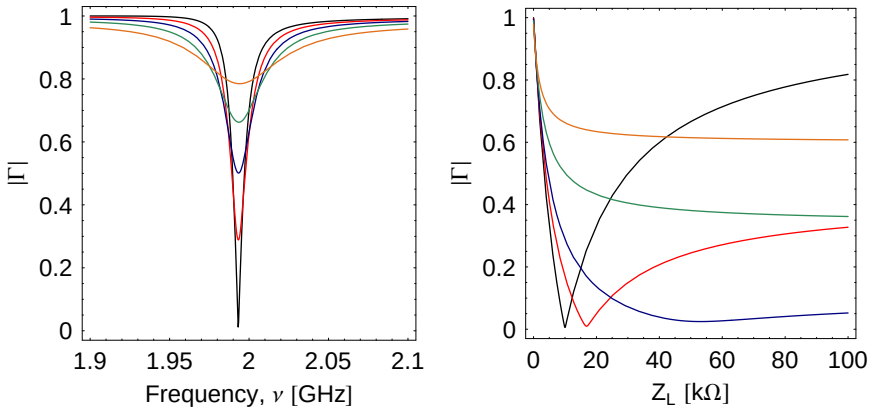

Figure 21: Effect of α, the attenuation constant of lossy transmission lines, on the reflection coefficient $|\Gamma|$ of a transformer matched to Z_L^0=10 kΩ at ν_0=2 GHz. Left: versus frequency ν, for α={black=0, red=.1, blue=.25, green=.5, yellow=1}. Right: versus load Z_L, at $\nu = \nu_0 = 2$ GHz, for α={black=0, red=.05, blue=.1, green=.25, yellow=.5}.

components. A small line-in leads to the junction. The stub and line lengths are begun from the bottom- and right-most ends of the junction, respectively. The stub terminates in an open, as required by the theoretical design. In the pictured setup, the line is terminated by a potentiometer; this potentiometer may also be left out to test the transformer with an open-circuited load.

Note that the input line to the potentiometer is soldered at a point slightly inwards from the end of the line, lending it an effective electrical length shorter than the intended design. This problem was fixed for the actual measurements by shortening the input line and soldering it as close as possible to the edge of the transformer. This process also minimizes the stray capacitance and inductance due to the connecting wire.

The system for measuring the DC resistance of the system is the same described as in the lumped element section: to wit, a bias tee with right-angle SMA connection to an SMA-BNC converter for an ohmmeter readout (see Fig. 13).

3.2.2 Results

The following results are reported for a distributed element impedance transformer with nominal match to $Z_L^0 = 1$ kΩ at $\nu_0 = 2$ GHz. Figure 23 shows experimental data for this transformer in an open-circuited configuration, i.e. $Z_L \to \infty$. A surprisingly good match is observed very close to the designed operating frequency of 2 GHz. This indicates that the transformer is matching strongly to internal losses. The quality factor of this open-circuited resonance is determined from a Lorentzian fit in Mathematica to be $Q_{\rm tot} = 34$. In the open-circuit regime Eqs. (21) and (27) thus give $Q_{\rm int} = 34$.

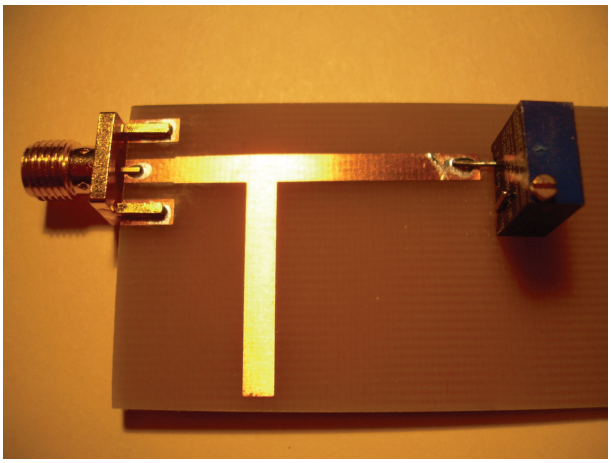

Figure 22: An example of a distributed element PCB transformer. Left to right: SMA connector with compensating structure, stub, and microstrip line-in attached to a potentiometer acting as a variable load impedance Z_L.

Figure 24 shows the open-circuited distributed element impedance transformer reflection coefficient data overlaid with the analytical model in Eq. (43), transformed to the lossy transmission line case in accordance with Eq. (44). Here, two formulas for contributions to the loss coefficient α, given in [6], are used:

$$\alpha_{\text{diel}} = 20\frac{\pi}{\log 10}\frac{\epsilon_{\text{eff}} - 1}{\epsilon_{\text{r}} - 1}\frac{\tan\delta}{\lambda}, \tag{46}$$

where α_{diel} is the contribution to α due to dielectric losses, ϵ_{r} is the dielectric constant relative to vacuum of the substrate, ϵ_{eff} is the effective relative dielectric constant of the transmission line geometry, $\tan\delta$ is the loss tangent of the substrate, and λ is the wavelength of the probing wave; and

$$\alpha_{\text{cond}} = 10\ R_{\text{S}}\ \frac{\left(\frac{8d}{W} - \frac{W}{4d}\right)\left(1 + \frac{d}{W} + \frac{d}{W}\frac{1}{\pi}\log 2\frac{d}{t}\right)}{\pi\ \log 10\ d\ Z_0\ \exp\frac{Z_0}{60}}, \tag{47}$$

where α_{cond} is the contribution to α due to conductive losses, d is the substrate thickness, W is the center conductor width in the microstrip transmission line geometry, t is the thickness of the metallization of the center conductor, $Z_0 = 50\Omega$ is the standard microwave frequency line impedance, and R_{S} is the surface resistivity given by

$$R_{\text{S}} = \sqrt{\frac{\omega\mu}{2\sigma}}, \tag{48}$$

with $\omega = 2\pi\nu$ the operating angular frequency, μ the permeability of the material taken to be μ_0 the vacuum permeability, and σ the bulk conductivity. The total modeled α is then given by

$$\alpha_{\text{tot}} = \alpha_{\text{diel}} + \alpha_{\text{cond}}. \tag{49}$$

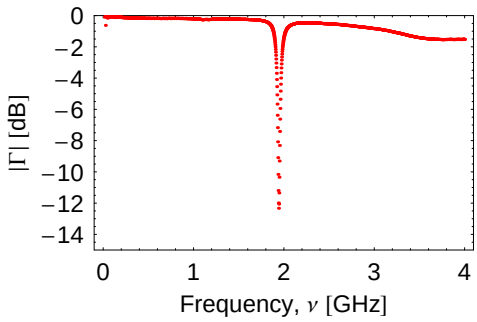

Figure 23: Experimental data for a distributed element impedance transformer with nominal match to $Z_L^0 = 1$ kΩ at $\nu_0 = 2$ GHz, open-circuited. Note the good match to internal losses.

The left panel of Fig. 24 shows the fundamental harmonic of the impedance transformer, overlaid with the theoretical fit. The parameters modified are the relative dielectric constant of the substrate, $\epsilon_{\mathrm{rFR4}} = 4.65$, with a corresponding $\epsilon_{\mathrm{eff}} = 3.53$, and its loss tangent $\tan\delta = .003$. These are modified from the manufacturer-supplied reference values $\epsilon_{\mathrm{rFR4}} = 4.65$ and $\tan\delta_{\mathrm{FR4}} = .015$. The good fit with different material parameters highlights the unreliability of FR4 as a substrate for microwave applications due to variations in parameter values [2]. A move to a substrate with favorable parameter values (i.e. lower loss tangent $\tan\delta$) and less variation in parameters from sample to sample would improve experimental conditions.

The right panel of Fig. 24 shows reflection coefficient data from the open-circuited $Z_L^0 = 1$ kΩ at $\nu_0 = 2$ GHz distributed element impedance transformer, plotted through 10 GHz. The higher harmonics in both the data and the analytical fit are visible. Clearly, there are far more losses experienced in the experiment which are not taken into account by the two loss sources described by α_{diel} and α_{cond}. These would include losses and stray reactive components due to the measurement setup, such as the SMA-PCB connector. Thus the analytical fit can only be trusted in a small frequency range over which the losses are adequately described by the chosen formulas for α. Ideally, however, one may wish to perform a measurement of the losses in the transmission line for accurate modeling and characterization.

4 Half-Wavelength Resonators

Half-wavelength resonators are resonant structures based on a transmission line design. Their main usefulness from the perspective of this report is an analytically determined quality factor Q in terms of the losses inside the transmission line. This allows the measurement of internal losses in a chosen transmission line and thus theoretical modeling of results from distributed element impedance

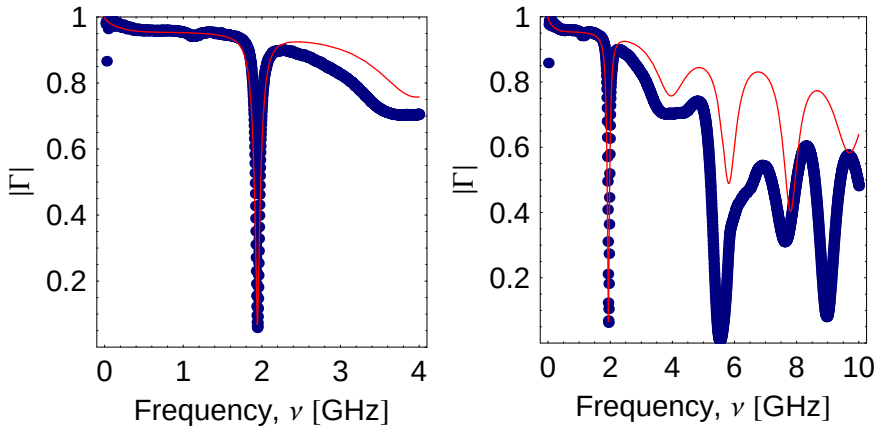

Figure 24: Experimental data overlaid with the lossy theoretical model of $|\Gamma|$. Blue=data, red=model. Left: The fit to the fundamental harmonic, ν_0=2 GHz. Right: The same fit, plotted until 10 GHz.

transformers. In addition they can be used to investigate the temperature dependence of these losses. The theory behind these resonators, restricted in this report to open-circuited half-wavelength resonators, and results from measurements performed on them in the course of this project are reported below.

4.1 Theory

4.1.1 Input Impedance and Quality Factor

An analytical expression for quality factor Q of an open-circuited, half-wavelength resonator is obtained by considering its input impedance about the resonance and mapping this to the input impedance about resonance of a lumped element parallel LRC circuit.

To begin, the input impedance of a parallel LRC circuit is given as

$$Z_{LRC\|} = (\frac{1}{R} + \frac{1}{\imath\omega L} + \imath\omega C)^{-1}. \tag{50}$$

About the resonance ω_0, we write

$$\omega = \omega_0 + \Delta\omega. \tag{51}$$

For $\Delta\omega \ll \omega_0$, Eq. (50) may be approximated as

$$Z_{LRC\|} \approx \frac{R}{1 + \imath 2Q\frac{\Delta\omega}{\omega_0}} \tag{52}$$

where $Q = \omega_0 RC$ as derived for the parallel LRC case.

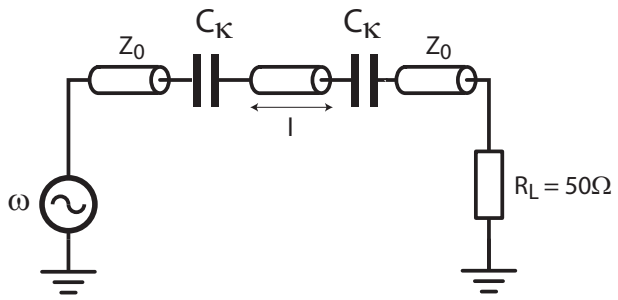

Figure 25: Schematic of a measurement setup for an open-circuited half-wavelength resonator of length l.

Next, we write the input impedance of an open-circuited half-wavelength lossy transmission line,

$$Z_{\lambda_0/2} = Z_0 \coth(\gamma l) \tag{53}$$

where γ is defined as in Eq. (45) and l is the length $\lambda_0/2$. Using the approximation in Eq. (51) and assuming small losses, we approximate the half-wavelength resonator input impedance as

$$Z_{\lambda_0/2} \approx \frac{Z_0}{\alpha l + \imath\pi \frac{\Delta\omega}{\omega_0}}. \tag{54}$$

A detailed derivation of both the above approximations is given in [4].

The identical algebraic form of the near-resonance input impedances given above allows a mapping of the half-wavelength resonator parameters to effective LRC values. These are given by

$$R = \frac{Z_0}{\alpha l} \tag{55}$$

$$C = \frac{\pi}{2\omega_0 Z_0} \tag{56}$$

$$L = \frac{2Z_0}{\pi\omega_0} \tag{57}$$

Thus

$$Q = \omega_0 RC = \frac{\beta_0}{2\alpha}, \tag{58}$$

where β_0 is given in Eq. (37). Since Q is a measurable of the resonator system, Eq. (58) allows calculation of α, and thus quantification of the degree of loss in the chosen transmission line design. Further details are available in [7].

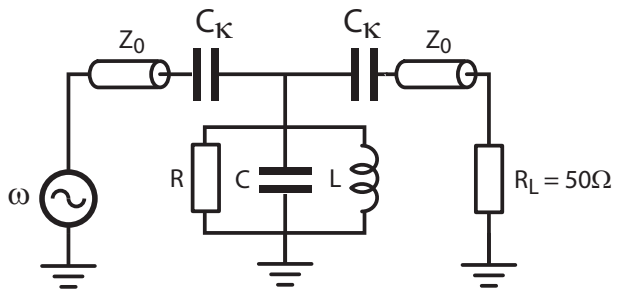

Figure 26: Schematic of the measurement setup with the open-circuited half-wavelength resonator mapped to lumped elements.

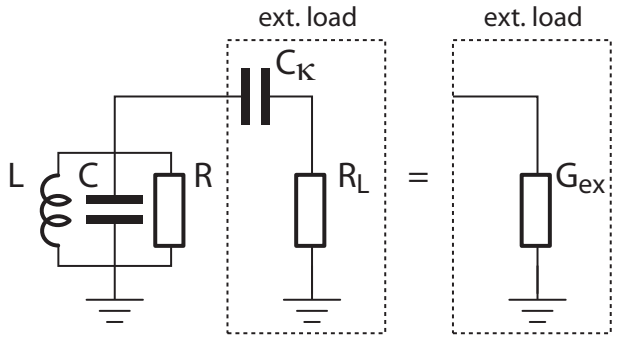

Figure 27: The effective external load conductance G_{ext} presented by the coupling capacitor C_κ and load impedance R_L=50 Ω.

4.1.2 Coupling and External Q

Physically realized half-wavelength resonators cannot be perfectly isolated systems because, as a matter of design, a method of coupling energy into the resonator is required. A schematic of the measurement setup is shown in Fig. 25. Here, a signal at frequency ω travels through a transmission line of characteristic impedance Z_0 which is coupled through the capacitance C_κ to the resonator of length l. In principle, this is all that is required, and the reflection coefficient Γ could be measured. However, since the resonator effectively filters out frequencies far from the resonance, the transmission of a two-ported resonator contains less noise than the reflection of a one-ported resonator. Therefore, the transmission T is the preferred measurable for this system. The circuit thus continues after the resonator of length l to another coupling capacitor C_κ, coupled to a transmission line of characteristic impedance Z_0 which is matched to R_L=50 Ω by the measurement system (i.e. a network analyzer). The same setup is shown in Fig. 26 with the resonator mapped to a lumped element parallel LRC circuit.

The external coupling presents new dissipative elements to the resonator system. Therefore the Q measured will be not only due to the internal Q of the

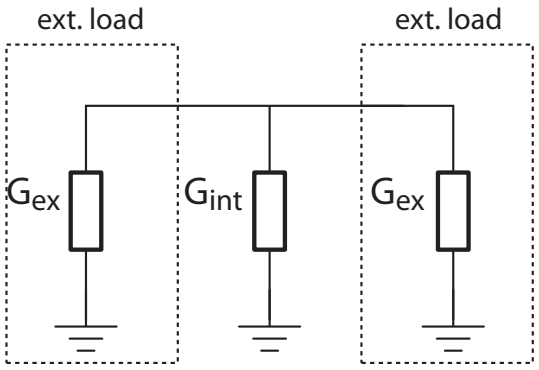

Figure 28: The effective external load conductance G_{ext} present in both input and output branches of the measurement system.

resonator, Q_{int}, but also to the dissipation due to external loading, Q_{ext}. Since Q_{int} is unknown and the measured quantity is Q_{tot}, Eq. (25) and 27 require an appropriate choice of Q_{ext} for a measurement dominated by the quantity of interest, Q_{int}. We thus require a calculation of Q_{ext} and its dependencies on circuit parameters; in particular, the only free parameter of the external loading is the capacitance, C_κ.

The effective external load conductance G_{ext} is schematically shown in Fig. 27. The effective resistive dissipation due to G_{ext} can be calculated as

$$R_{\text{ext}} = \frac{1}{G_{\text{ext}}} = \frac{1 + \omega^2 C_\kappa^2 R_L^2}{\omega^2 C_\kappa^2 R_L}. \tag{59}$$

This is combined in parallel with R to give the total dissipation in the circuit. Because transmission is measured and this requires two branches, each with load conductance G_{ext} as shown in Fig. 28, the total dissipation is halved. By Eq. (25), we can consider the external dissipation separately and use it to calculate Q_{ext}, to be subsequently added to the known Q_{int}. Since both Q's are due to parallel dissipative components, we use Eq. (21) to calculate the external Q with the capacitive resonator mapping for C in Eq. (56) and finally divide by 2 for the symmetric coupling to obtain

$$Q_{\text{ext}} = \frac{\pi}{4Z_0}\left(\frac{1}{\omega^2 C_\kappa^2 R_L} + R_L\right) \tag{60}$$

More details are available in [7].

With the equation for Q_{ext} as a function of C_κ, design of half-wavelength resonators with calculable Q_{int}'s and thus α's is realizable. In making the choice of what values of C_κ to use, the issue lies in ensuring that the resonator is not too under-coupled, such that it lacks enough input energy to make the resonance easily measurable (i.e. compared to noise), and not too over-coupled, such that the measurement consists almost solely of Q_{ext} as in Eq. (26). In principle,

however, Q_{int} is not known, and thus it is necessary to construct a range of C_κ values to ensure the possibility of a good measurement.

4.1.3 Insertion Loss

Theoretically, Q_{int} can be calculated from the measured Q_{tot} and the calculated Q_{ext} based on the constructed C_κ. The coupling capacitance C_κ, however, is known only from simulations done, for this project, in Maxwell. Experimental realities such as variations in the etching process and in the material dielectric constant ϵ_{r} may alter this value. Thus it is desirable to calculate Q_{ext} with purely measured values to eliminate theoretical assumptions.

To do so, we use the insertion loss L_0, a measurable of the system. Defining the coupling coefficient g,

$$g \equiv \frac{Q_{\text{int}}}{Q_{\text{ext}}} = \frac{G_{\text{ext}}}{G_{\text{int}}} = \frac{R}{R_{\text{ext}}}, \tag{61}$$

the insertion loss can be rewritten as

$$L_0 = \frac{g}{g+1}. \tag{62}$$

Equations 25, 61 and 62 can be combined to obtain

$$Q_{\text{int}} = \frac{1}{1-L_0} Q_{\text{tot}} \tag{63}$$

$$Q_{\text{ext}} = \frac{1}{L_0} Q_{\text{tot}}. \tag{64}$$

The internal and external quality factors of the resonator system can then be calculated from the insertion loss and total quality factor, both measurable quantities.

4.2 Experiment

To gauge the losses in the PCB transmission lines and their temperature dependence, PCB microstrip resonators have been fabricated and measurements at room temperature and 77 K have been performed. The design and results are reported below.

4.2.1 Design

Figure 29 shows the PC Board microstrip half-wavelength resonator, designed for ν_0=2 GHz, used for the following measurements. The connection is achieved with SMA connectors with the manufacturer-provided compensation structure, followed by a short feedline. This is coupled to the half-wavelength resonator, a piece of microstrip with a 50 Ω designed impedance, via 1mm wide gap capacitors. The capacitance of these gaps has been calculated in Maxwell to be

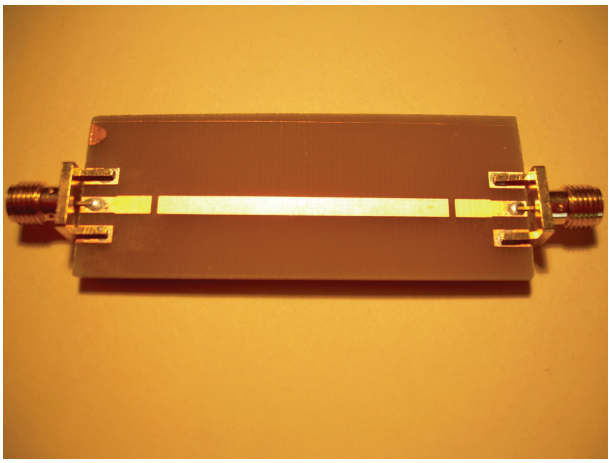

Figure 29: An example of a realized PCB half-wavelength resonator designed for ν_0=2 GHz. Note the 1mm gap capacitors.

	$T_{\max}$	Q_{tot}	Q_{ext}	Q_{int}	α
Room $\approx$ 300 K	.043	43.7	1016	45.7	0.86
LN2 $\approx$ 77 K	.151	99.7	660	117.4	0.33

Table 2: Resulting data for the PCB half-wavelength resonator with 1mm gap capacitors at room temperature and in liquid nitrogen.

48 fF, yielding $Q_{\text{ext}} = 864$. This is appropriately large given the internal Q's measured in the distributed element transformers.

For room temperature measurement, coaxial cables are attached to the network analyzer and the resonator. For measurement at 77 K in liquid nitrogen (LN2), semi-rigid cables manufactured in the laboratory are connected to the coaxial cables and the resonator. These can be placed inside a small liquid nitrogen dewar for cooling the device.

4.2.2 Results

Figure 30 shows the transmission magnitude $|T|$ graphed about the fundamental resonance for the $\nu_0 = 2$ GHz PCB half-wavelengthvresonator with 1mm wide gap capacitors. There is a clear improvement in the quality of the resonance between the room temperature 300 K (left panel) and liquid nitrogen 77 K (right panel) measurements. The peak transmission is observed to more than triple from high to low temperature.

Table 2 shows the measurement data and corresponding results for the two measurements. The calculation of Q_{tot} is performed via the fits-to-data shown in Fig. 30. Q_{ext} and Q_{int} are then calculated via Eqs. (64) and (63). Eq. (58) is used to calculate the α at resonance.

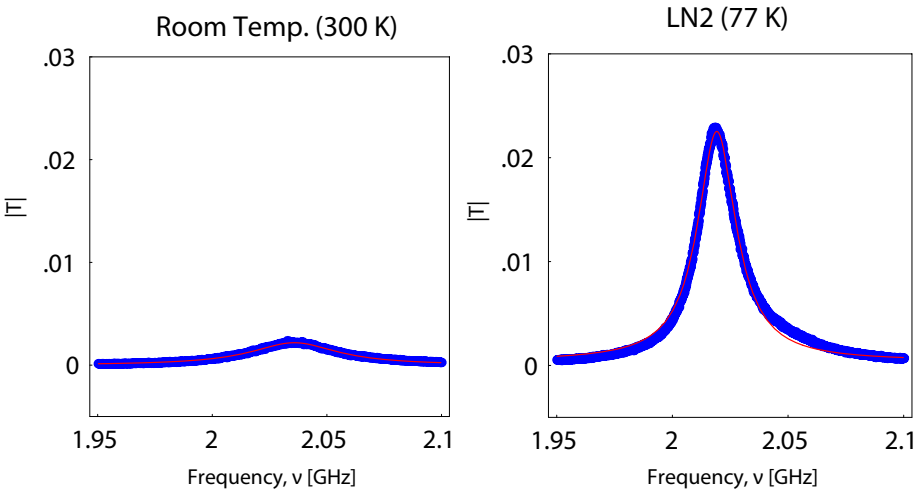

Figure 30: Magnitude of the transmission $|T|$ for a PCB half-wavelength resonator operating at $\nu_0 = 2$ GHz with 1mm gap capacitors for $C_\kappa = 48$ fF and a theoretical $Q_{\text{ext}} = 864$. Left: room temperature ≈ 300 K. Right: Liquid nitrogen (LN2) ≈ 77 K. Both plots: blue dots are data, red line is a Lorentzian fit.

Q_{int} is seen to increase by a factor of 2.6 during the temperature drop, with a corresponding drop in the internal loss α of the same factor. This result confirms the important temperature dependence of the losses, which allows a mechanism by which to increase the quality factor of the transmission line resonances. This can be used to make impedance transformers that match to higher loads Z_L^0. Thus low temperatures provide a method by which to increase matched loads, operating frequencies and therefore also bandwidth for making fast impedance transformers.

5 Silicon Chips

The impedance transformers analyzed in this report have been demonstrated to contain intrinsic losses that hamper the ability to match to high loads at high frequencies. To increase flexibility in this respect, transformers must be fabricated for which helium-temperature cooling is possible. The microstrip design formulas indicate that an increase in dielectric constant of the available substrate would allow for smaller transformer dimensions. Silicon chips provide an answer by allowing miniaturization and providing an increase over the FR4 dielectric constant of a factor of more than 2, from $\epsilon_{rFR4} = 4.5$ to $\epsilon_{rSi} = 11.9$.

Silicon chips also make possible the use of superconducting materials. Superconducting half-wavelength resonators have been demonstrated to exhibit quality factors of order 10^5 [7]. The move to silicon chips thus allows for the greatest

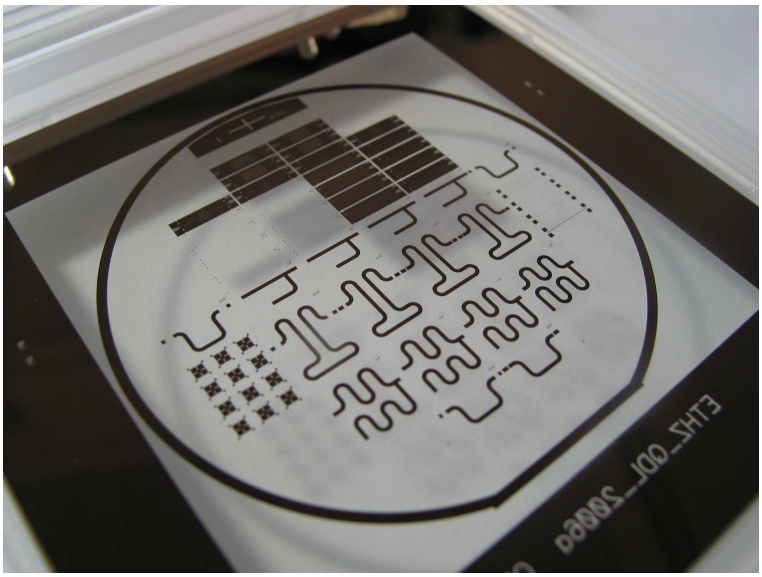

Figure 31: The optical mask for the silicon chip impedance transformers and half-wavelength resonators.

flexibility in reducing internal losses in the distributed element impedance transformers and in achieving the goals of high frequency molecular electronics.

5.1 Optical Mask Design

The design for the optical mask necessary for lithographic or electron beam fabrication is show in Fig. 31. The base chip size, indicated by the intersections of the blue dicing lines, is 2mm x 7mm. The yellow microstrip designs are immediately seen to be designed in multiples of this base chip size. The reasons for this and for the design of the coplanar waveguide (CPW) chips seen in red are elucidated below.

Four matched loads Z_L^0 were decided upon: 10^3, 10^4, 10^5, and 10^6 Ω. These choices allow testing of low resistances up through the quantum resistance and resistances observed in single-molecule junctions. Operating frequencies are chosen and described below.

A labeling system is utilized. For the impedance transformers, it consists of transmission line type, n where $Z_L^0 = 10^n\Omega$, and the operating frequency ν_0 in GHz. For a microstrip transformer with Z_L^0=1 kΩ and ν_0=2 GHz the chip label is "M23". For a CPW transformer with Z_L^0=10 kΩ and ν_0=1.5 GHz the chip label is "C154". Labeling for the half-wavelength resonators has the same first two terms plus a Q followed by the order of Q_{ext}. A CPW resonator for ν_0=1.5 GHz and Q_{ext} of order 10^5 the label is "C15Q5". The register mark chips have the marking of their parent chip (explained in the CPW section)

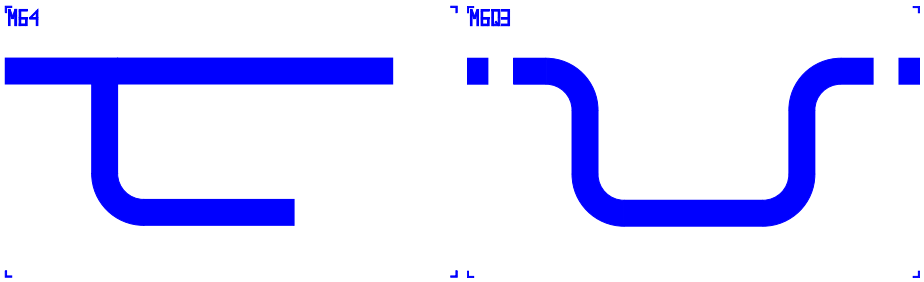

Figure 32: Microstrip silicon chip designs for ν_0=6 GHz. Left: Impedance transformer for Z_L^0=10 kΩ. Right: Half-wavelength resonator for Q_{ext} of order 10^3.

Chip Label	ν_0 [GHz]	Gap size [μm]	C_κ [fF]	Q_{ext}
M6Q2	6	100	32.7	200
M6Q3	6	400	10.1	2168
M6Q4	6	600	5.4	7581
M6Q5	6	800	4.7	10137
M2Q2	2	50	43.3	1062
M2Q3	2	100	32.7	1795
M2Q4	2	300	14.3	9730
M2Q5	2	600	5.4	68226

Table 3: Microstrip half-wavelength resonator designs for the silicon chip optical mask. C_κ is calculated with Maxwell assuming 200nm of oxidized silicon (SiO_x) in the substrate. Q_{ext} is calculated with Eq. (60).

followed underneath by an "R".

Note that while the microstrip designs are laid down as a positive layer, where outlined geometry represents metallization, the coplanar waveguide designs are drawn negatively, where outlined geometry represents metallization to be removed.

5.1.1 Microstrip Designs

For the microstrip chips, two sets of impedance transformers were designed: for operation at 2 GHz (Fig. 33) and 6 GHz (Fig. 32). These were chosen to fit within the operating bands of most of the laboratory equipment for low-temperature operation, such as amplifiers, circulators and directional couplers. Half-wavelength resonators are designed for each of these operating frequencies, with four different coupling capacitances for appropriate variation in the order of Q_{ext}, allowing for measurements from the high-loss, room-temperature range to the small loss, superconducting regime. Table 3 displays the resonator operating frequency ν_0, approximate order of Q indicated on the chip label, chosen

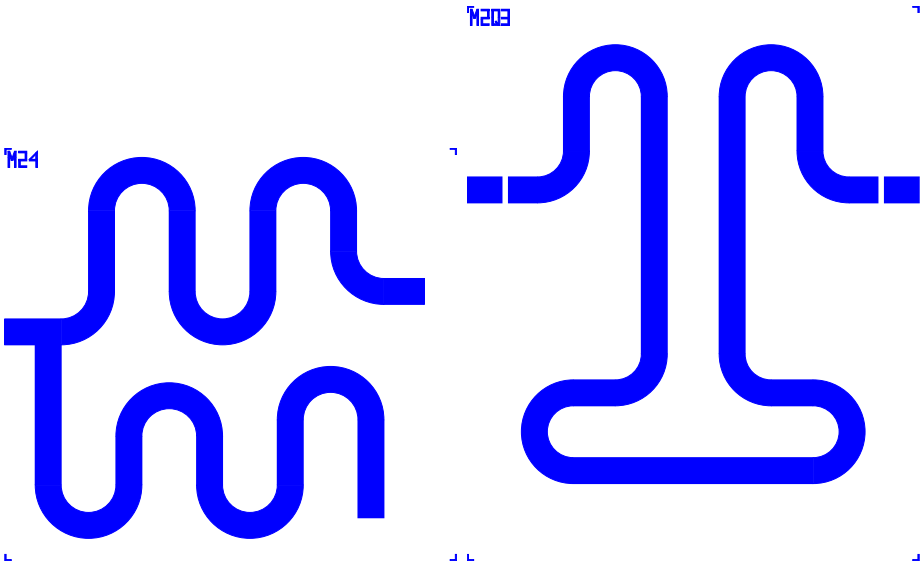

Figure 33: Microstrip silicon chip designs for ν_0=2 GHz. Left: Impedance transformer for Z_L^0=10 kΩ. Right: Half-wavelength resonator for $Q_{\rm ext}$ of order 10^3.

microstrip resonator gap capacitor sizes, corresponding C_κ, and resulting $Q_{\rm ext}$. Note that the C_κ calculations performed in Maxwell assume a 200 nm thick layer of silicon oxide, SiO_x, formed by thermal oxidation of the silicon substrate.

The disadvantages of the microstrip transmission line design became immediately evident upon design. To match to the standard microwave frequency operating impedance 50 Ω the width of the microstrip line is fixed as a function of the thickness and dielectric constant ϵ_r of the substrate [2, 4]. The fixed width of microstrip lines puts an upper limit on their turning radius, preventing efficient size reduction of on-chip designs. This forces the use of multiple base chip sizes as well as the use of all the area available, up until the chip edges. A number of problems now appear: the microstrip lines in these chip designs are typically separated by at most two multiples of their width, which will likely lead to interline coupling. They are also exposed to the chip edge, which changes the effective dielectric constant $\epsilon_{\rm eff}$. Also, because of their fixed width, there is no method to minimize reflections at the transition from sample holder input lines to chip launcher.

Additionally, fabricating break junctions, nanowires, or other structures necessary for accessing quantum systems is made more difficult by the fact that the ground plane for the microstrip lines is on the opposite side of the transmission line itself. Thus a nanowire at the edge of the loaded line of one of the silicon chip microstrip impedance transformers would have to be connected to ground either by a 'via' to the opposite chip side, a difficult prospect for silicon chips, or by wrapping around the chip edge to the opposite chip side, also an impractical

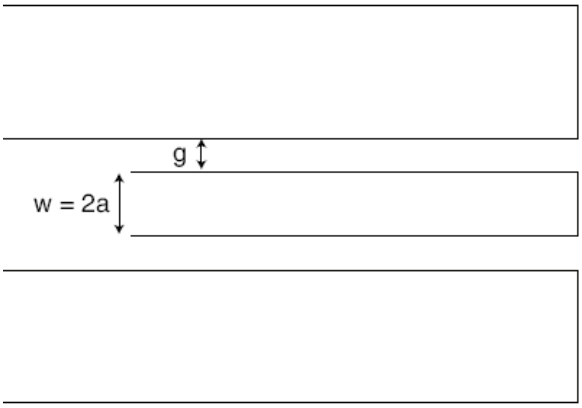

Figure 34: The coplanar waveguide (CPW) transmission line. The center conductor width is $w = 2a$, and g is the gap width.

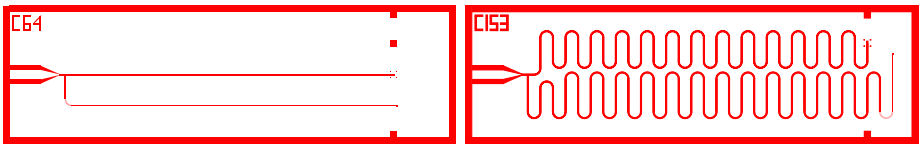

Figure 35: Two CPW impedance transformers. Left: ν_0=6 GHz, Z_L^0=10 kΩ. Right: ν_0=1.5 GHz, Z_L^0=1 kΩ.

idea for silicon chips. The long length of such a nanowire would also increase the stray inductance and capacitance of the effective load.

These difficulties make clear that a different transmission line design could be advantageous. The choice made was the coplanar waveguide, described in the following section.

5.1.2 Coplanar Waveguide (CPW) Designs

The coplanar waveguide design is show in Fig. 34. Here, the center conductor of width $w = 2a$ projects fields lines through the gap of width g to the lateral ground planes. One of the potential issues identified with the CPW design stems from the lateral ground planes, which when used on a chip with a back metallization for the ground plane becomes a floating ground. Better grounding is achieved by attaching vias from the lateral floating grounds to the back ground plane. Modes in the lateral ground planes may also be excited; these may be suppressed with a chosen periodicity of via placement.

The impedance match to the standard microwave operating impedance of 50 Ω is achieved in the CPW case by adjusting the ratio of center conductor width

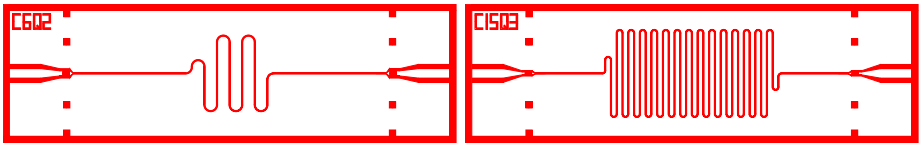

Figure 36: Two CPW half-wavelength resonators. Left: ν_0=6 GHz, Q_{ext} of order 10^2. Right: ν_0=1.5 GHz, Q_{ext} of order 10^3.

Figure 37: The end of the loaded branch of a CPW impedance transformer. Visible is the 30 μm long end-gap.

to gap width, w/g. Thus unlike the microstrip design, the CPW transmission line cross sectional size can be arbitrarily tailored for convenience, up to the resolution of the fabrication system. This allows for a far smaller turning radius and hence the ability to easily squeeze long lengths of transmission lines onto smaller chip dimensions. It also allows for the minimization of reflections at the transition from sample holder input line to chip launcher by allowing the launcher to begin at the input line width and to subsequently shrink (at constant impedance) to the on-chip line width. These transitions are visible at the lateral edges of the chips. For these chips, a center conductor width of $w = 10\mu m$ was chosen. Note also that all the CPW designs fit on one base chip size of 2 mm x 7 mm, with ample space to avoid edge proximity and interline coupling.

The CPW chips provide another advantage by their use of lateral ground planes. The end of the loaded line of the impedance transformer is directly opposite the ground. Thus attachment of a nanowire or other nanoscale load with small stray reactances is made potentially simpler as the device has only to reach across the 30 μm long end-gap to be grounded. The length of the end-gap is chosen to minimize stray capacitance due to center conductor-ground coupling at the edge while providing a convenient length for future nanowire deposition. The condition on minimization is that $l_{\text{end}} > 2(2g + w)$ where l_{end} is the end-gap length [5].

Because of the small chosen center conductor width of 10 μm, it is difficult to achieve high coupling capacitances C_κ with gap capacitors as in the microstrip half-wavelength resonator case. To increase the available C_κ and decrease Q_{ext} for higher-loss measurements, finger capacitors are used. Note that the use of these are possible only because of the dependence of CPW impedance on the center conductor-to-gap ratio. Figure 38 shows one such finger capacitor. The fingers increase the exposed conductor area and thus the capacitance of the gap. They will also modify the effective length of the resonator, since the resonator end is less well-defined. This extra length, however, is negligible compared to

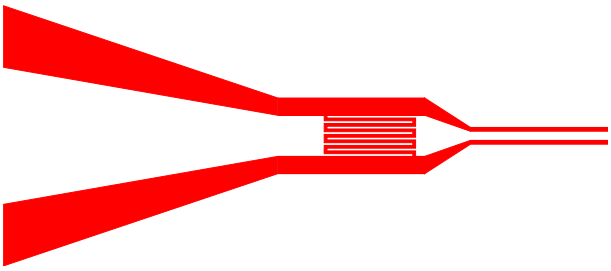

Figure 38: A multi-finger capacitor for launcher-resonator coupling in the CPW half-wavelength resonator.

Chip Label	ν_0 [GHz]	C_κ [fF]	Q_{ext}
C6Q2	6	79.8	35.5
C6Q3	6	12.7	1362.7
C6Q4	6	4.6	10492.9
C6Q5	6	1.4	117774.0
C15Q2	1.5	178.4	111.9
C15Q3	1.5	43.0	1913.6
C15Q4	1.5	12.7	21791.4
C15Q5	1.5	4.6	167874.0

Table 4: CPW half-wavelength resonator designs for the silicon chip optical mask. C_κ is calculated with Maxwell assuming 200nm of oxidized silicon (SiO_x) in the substrate. Q_{ext} is calculated with Eq. 60.

the entire resonator length and should only result in a small resonance shift.

Table 4 displays the chosen CPW C_κ values and resulting Q_{ext}. Note that the C_κ calculations performed in Maxwell assume a 200 nm thick layer of silicon oxide, SiO_x due to oxidation of the silicon substrate.

Figure 39 shows two registration mark chips. The registration marks are positioned at the location of the end-gaps. These chips will be used as alignment marks for a gold-sputtering fabrication process by which the nano-scale wiring for quantum device connection will be first laid down, and then the impedance transformer built on top by optical or electron beam lithography.

Figure 39: Two registration mark chips for quantum device fabriaction. Left: ν_0=6 GHz, Z_L^0=1 kΩ. Right: ν_0=1.5 GHz, Z_L^0=1 kΩ.

6 Conclusions and Future Work

In this project, impedance transformation circuits for high bandwidth measurements of molecules and other quantum electronic systems at high frequencies have been investigated. Such impedance transformers could enable sensitive and efficient measurements of quantum electronic devices on nanosecond timescales.

For transformer development and testing, PC Board circuits were examined. Both discrete and distributed element impedance transformers were measured at room temperature, and studies of loss mechanisms were performed at low temperature.

The lumped element PC Board circuits based on surface-mount devices were shown to exhibit substantial stray loss and reactive components. Reactive components such as stray inductance and capacitance shift matched loads and operating frequencies; stray loss components prevent matching to high loads at high frequencies with high bandwidth and sensitivity. Distributed element circuits were shown to be less susceptible to stray reactance, but limited by losses in the materials. These losses could be reduced by manufacturing distributed element transformers with superconductors for low temperature operation.

The material losses of the PC Board impedance transformers were investigated at low temperature to explore the limits of distributed element circuit operation. PC Board half-wavelength resonators were built and measured at room temperature (300 K) and liquid nitrogen temperature (77 K), demonstrating a decrease in losses of more than a factor of 2. These results indicate that the use of low temperatures and low-loss materials will enable the construction of matching circuits for higher loads with better-controlled sensitivity.

Analytical and numerical tools to analyze our experimental results were also developed. Using these tools we have been able to determine stray reactive and dissipative components in the matching circuit as well as reactive components in the load. These tools will be valuable for detailed analysis of measurement data on quantum electronic circuits to be performed in the future.

To begin fabrication of low loss circuits, an optical mask for lithographic fabrication of silicon chip impedance transformers was designed. The mask allows for the parallel fabrication of a large number of silicon chip impedance transformers for high matched loads. The high dielectric constant of the silicon (ϵ_r=11.9) compared to FR4 (ϵ_r=4.5) allows for device miniaturization, as well as providing a low-loss microwave substrate with less variation from sample-to-sample. Both microstrip and coplanar waveguide transmission line designs are included on the optical mask. Coplanar waveguides offer increased versatility compared to microstrip due to their modifiable width for a fixed impedance. Their geometric flexibility and use of lateral ground planes also allow for easier future integration of quantum electronic devices.

This project has laid the groundwork for the development of fast, high-frequency impedance transformers for molecular electronics. This will include studies of low-loss, silicon chip transformer implementations at liquid helium (4.2 K) and dilution refrigerator ($\sim$ 20 mK) temperatures. Ultra-low loss impedance transformers will be realized with the use of superconductors, which

allow for quality factors on the order of 10^5 by eliminating much of the conductor losses. Ultra-reduced losses allow for operation at higher frequencies, which in turn allows for the creation of higher bandwidth, faster impedance transformers. Ultimately, this development will enable fast and sensitive measurements of molecular electronics and other nanoscale quantum electronic systems.

References

[1] G. Cuniberti, G. Fagas, and K. Richter, *Introducing molecular electronics*, Springer, 2005.

[2] T. C. Edwards and M. B. Steer, *Foundations of interconnect and microstrip design*, Wiley, 2000.

[3] H. Park, A. Lim, J. Park, A. Alivisatos, and P. McEuen, *Fabrication of metallic electrodes with nanometer separation by electromigration*, Applied Physics Letters **75** (1999), no. 2, 301–303.

[4] David M. Pozar, *Microwave engineering*, Addison-Wesley Publishing Company, 1990.

[5] Rainee N. Simons, *Coplanar waveguide circuits, components, and systems*, Wiley, 2001.

[6] Brian C. Wadell, *Transmission line design handbook*, Artech House, 1991.

[7] A. Wallraff, *Superconducting solid state cavity quantum electrodynamics*, unpublished, 2003.